

First-principles study of structural, elastic and electronic properties of NdTe₂ and TiNdTe₂

Y. MOGULKOC^{a*}, Y.O. CIFTCI^b, M. KABAK^a, K. COLAKOGLU^b

^a *Department of Physics Engineering, Ankara University, 06100, Ankara, Turkey*

^b *Department of Physics, Gazi University, 06500, Ankara, Turkey*

Received: 25.04.2013; Accepted: 15.05.2013

Abstract. The first-principles calculations of structural, elastic and electronic properties of NdTe₂ (C38) and TiNdTe₂ (L2₁) compounds are investigated using the methods of density functional theory within the generalized gradient approximation (GGA) based on exchange-correlation energy optimization. We have calculated the lattice constants, bulk modulus and its pressure derivative agrees with the available experimental data. We have investigated the elastic properties to obtain further information. Second-order elastic constants, Zener anisotropy factor, Poisson's ratio, Young's modulus, isotropic shear modulus, B/G ratios and Kleinman parameter are calculated in this study. Electronic band structures are investigated using the total and partial density of states, charge distribution and electronic localization function.

Key words: *ab initio* calculation; elasticity; electronic structure; electronic density of states

1. INTRODUCTION

The rare-earth compounds have recently attracted special attention in many applications owing to their interesting physical, electronic, and mechanical properties that make them significant materials for technological and many areas of industrial applications [1-28]. The use of rare-earth compounds in technological applications has increased over the past years. Rare-earth compounds are used in many technological devices such as optoelectronic and communication devices. Recently, the semi-empirical quantum chemical models for the calculation of complexes of lanthanide ions are defined for neodymium. Several lanthanides such as neodymium are exhibited luminescence in the telecommunication low-loss near infrared regions of standard silica based optical fibers [28, 29]. Structural, elastic, electronic and thermodynamic properties of Nd₂Te via first principle calculations have been investigated by us [30]. The X-ray diffraction single-crystal structure analysis of NdTe₂ which is prepared by chemical vapor transport reactions in the presence of traces of iodine also revealed superstructure reflections in order that NdTe₂ crystallizes orthorhombic [31]. Experimental work of the TiNdTe₂ compound is studied by Godzhaev et al. [32].

* Corresponding author. *Email address:* mogulkoc@eng.ankara.edu.tr (Y. Mogulkoc)

Tel.: +90 312 2128577-2724; Fax: +90 312 2127343

<http://dergi.cumhuriyet.edu.tr/ojs/index.php/fenbilimleri> ©2013 Faculty of Science, Cumhuriyet University

First-principles study of structural, elastic and electronic properties

In this work, first-principles calculations within the framework of the density functional theory (DFT) have been processed [33, 34]. In calculations, plane-wave pseudopotential is used to obtain the equation of state (EOS) and related equilibrium quantities of the energy, the bulk modulus, derivative of bulk modulus of NdTe₂ and TlNdTe₂. In addition, in order to obtain further information about elastic properties, second-order elastic constants, Zener anisotropy factor, Poisson's ratio, Young's modulus, isotropic shear modulus, B/G, and Kleinman parameter of NdTe₂ and TlNdTe₂ have been calculated at zero pressure. The final section, electronic structure and electron localization function section, with all-electron calculations of band structure, PDOS and electron localization function (ELF) [35] of these compounds are investigated and related analysis are discussed.

2. METHOD of CALCULATIONS

The Vienna *Ab-initio* Simulation Package (VASP) code [36, 37] based on DFT is employed to examine the behavior of tetragonal (C38) structure of NdTe₂ and the Heusler structure (L2₁) of TlNdTe₂ compounds. The calculation is carried out with projector augmented wave (PAW) [38, 39] potentials are built within the generalized gradient approximation (GGA) [40]. In the present calculation, the potpaw GGA pseudopotentials of Nd, Te and Tl are used.

The equilibrium lattice parameters have been computed by minimizing the crystal total energy calculated for different values of lattice constant by means of Murnaghan's equation of state (eos) [41]. The wave functions are expanded in the plane waves up to a kinetic energy cut-off 650 eV. This cut-off value is found to be convenient for the electronic band structures. The Monkhorst and Pack grid of k-points used for integration in capable of being reduced part of the Brillouin zone are (12x12x8) and (12x12x12) of NdTe₂(C38) and TlNdTe₂(L2₁) compounds, respectively. The total energy is nearly seen to be independent of the number of k-points, expectedly if all our calculations in k-space are numerically well converged.

3. RESULTS and DISCUSSION

3.1. Structural and elastic properties

Crystal structures of NdTe₂ and TlNdTe₂ compounds are obtained using the energy minimization method. Calculated lattice constants, bulk modulus and its pressure derivative are presented in Table 1.

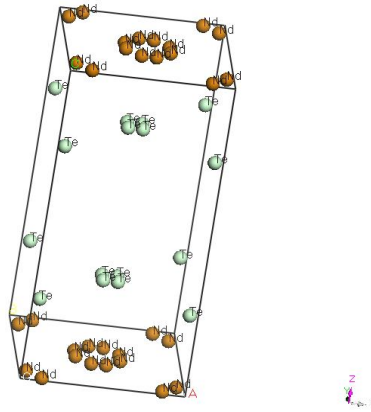
Table 1. The calculated lattice constants, bulk modulus (B) and its pressure derivative (B') of NdTe₂ and TiNdTe₂

Material	Structure	Reference	Lattice constant [Å]	B [GPa]	B'
NdTe ₂	Tetragonal (C38)	This work	a= 4.586 c=9.360	64.55	5.28
		Exp. ^a	a=4.419 c=9.021		
TiNdTe ₂	The Heusler (L2 ₁)	This work	a=7.95	46.58	4.36

^a: [28]

Our result for lattice constant of NdTe₂ is nearly 0.370% lower than the other experimental result for C38 crystal structure.

The related structures of these compounds are given in Figure 1 and 2 for NdTe₂ and TiNdTe₂, respectively.

**Figure 1.** A unit cell of NdTe₂

The crystal structure of NdTe₂ is given in Figure 1 in which the brown spheres are shown as Nd and the light green spheres are shown as Te.

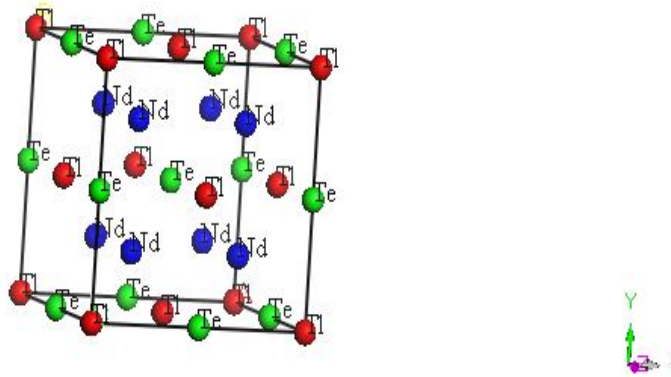


Figure 2. A unit cell of TlNdTe₂

The crystal structure of TlNdTe₂ is presented in Figure 2 in which Tl's are shown as red spheres, Nd's are shown as blue spheres, and Te's are shown as green spheres.

Elastic properties of materials are very important because of various fundamental solid state properties, such as Zener anisotropy factor, Poisson's ratio, Young's modulus, and shear modulus.

The elastic constants determine the response of the crystal to external forces and play a big role in specifying the strength of the materials. The elastic properties of these compounds are at zero pressure value using the basis of structural observations. There are two common methods [42-45] for obtaining the elastic constants through the ab-initio model of materials from their well-known crystal structures: an approach based on analysis of the total energy of properly strained states of the material in the volume conserving technique and an approach based on the analysis of changes in calculated stress values resulting from changes in the stress-strain technique. In this study, stress-strain method is used to obtain the second-order elastic constants (C_{ij}) that are calculated and presented in Table 2. The elastic constants of the crystal whose structure has been fully relaxed under a given set of exchange–correlation potential functions are calculated in which minimize the total energy of whole system. The Born's stability criteria's [46] should be satisfied for the stability of lattice. The known conditions for mechanical stability of cubic crystals are: $C_{11}>0$, $C_{11}-C_{12}>0$, $C_{44}>0$, $C_{11}+2C_{12}>0$ and

$C_{12} < B < C_{11}$. the mechanical stability criteria are $C_{11} > 0$, $C_{33} > 0$, $C_{44} > 0$, $C_{66} > 0$, $(C_{11} - C_{12}) > 0$, $(C_{11} + C_{33} - 2C_{12}) > 0$ and $2(C_{11} + C_{12}) + C_{33} + 4C_{13} > 0$ for tetragonal structure. These traditional mechanical stability conditions are investigated by using the calculated elastic constants for considered structures. The calculated values of C_{ij} are given in Table 2 for NdTe₂ and TiNdTe₂. The related mechanical stability conditions are satisfied for C38 structure in NdTe₂ and L2₁ structure in TiNdTe₂. Therefore, C38 structure in NdTe₂ and L2₁ structure in TiNdTe₂ are mechanically stable.

Table 2. The calculated second-order elastic constants (C_{ij}), Zener anisotropy factor (A), Poisson's ratio (ν), isotropic shear modulus (G), B/G and Kleinman parameter(ξ) of NdTe₂ TiNdTe₂ at zero pressure

Material	C_{11} [GPa]	C_{12} [GPa]	C_{44} [GPa]	A	ν	G [GPa]	B/G	ξ
NdTe ₂	81.09	56.29	37.39	3.02	0.32	13.99	4.614	0.781
TiNdTe ₂	79.47	30.19	15.88	0.64	0.31	18.95	2.459	0.521

The Zener anisotropy factor (A), Poisson's ratio (ν), Young's modulus (E), isotropic shear modulus (G) and Kleinman parameter (ξ) which are the most interesting elastic parameters for applications, are also calculated in terms of the computed by the following relations [47] and presented in Table 2.

$$A = \frac{2C_{44}}{C_{11} - C_{12}} \quad (1)$$

$$\nu = \frac{1}{2} \left[\frac{\left(B - \frac{2}{3}G \right)}{\left(B + \frac{1}{3}G \right)} \right] \quad (2)$$

where $G = (G_V + G_R)/2$ is the isotropic shear modulus, G_V is Voigt's shear modulus corresponding to the upper bound of G values and G_R is Reuss's shear modulus

corresponding to the lower bound of G values and can be written as $G_V=(C_{11}-C_{12}+3C_{44})/5$ and $5/G_R=4/(C_{11}-C_{12})+3/C_{44}$.

One of the distinct parameter is Kleinman parameter that describes the relative positions of the cation and anion sub-lattices under volume conserving strain distortions for which positions are not fixed by symmetry [48]. Kleinman parameter is defined as below

$$\xi = \frac{C_{11} + 8C_{12}}{7C_{11} + 2C_{12}} \quad (3)$$

Kleinman parameter value is found to be 0.781 for NdTe_2 and 0.521 for TlNdTe_2 .

The calculated elastic constants (C_{ij}), isotropic shear modulus (G), B/G , Zener anisotropy factor (A), Poisson's ratio (ν), Young's modulus (E) and Kleinman parameter are given in Table 2. Commonly used empirical relations are between bulk and isotropic shear modulus. Their brittle/ductile behaviors are determined with ratio of B/G . The present values of B/G are 4.614 for NdTe_2 and 2.459 for TlNdTe_2 . These values are higher than the critical value of 1.75. These results also support their ductile characters.

The Zener anisotropy factor A is a measure of the degree of elastic anisotropy in solids. The A takes the value of 1 for a completely isotropic material. If the value of A smaller or greater than unity it shows the degree of elastic anisotropy. The calculated Zener anisotropy factor is equal to 3.02 for NdTe_2 and 0.64 for TlNdTe_2 at 0 GPa, which indicates that these compounds are entirely anisotropic.

The Poisson's ratio provides more information about the characteristics of the bonding forces than any of the other elastic constants. Calculated Poisson's ratios are 0.32 for NdTe_2 and 0.31 for TlNdTe_2 . It shows that the inter atomic forces in NdTe_2 and TlNdTe_2 are central in nature.

3.2. Electronic properties

The calculated band structures and corresponding electronic density of state (DOS) of NdTe₂ (tetragonal) and TlNdTe₂ (the Heusler) structures along the high symmetry points in the first Brillouin zone are shown in Figure 3 and 4. The position of the Fermi level is set to 0 eV.

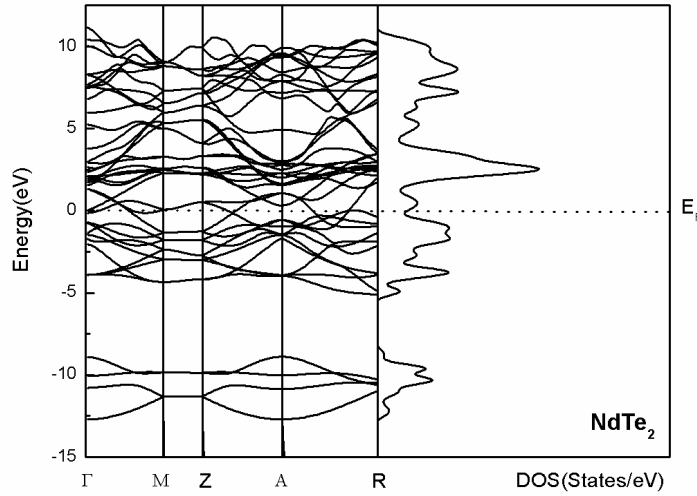


Figure 3. The energy bands and corresponding total DOS of NdTe₂

The calculated band structure and density of states of NdTe₂ (C38) is presented in Figure 3. The symmetry points are $\Gamma(0,0,0)$, $M(1/2,1/2,0)$, $Z(0,0,1/2)$, $A(1/2,1/2,1/2)$ and $R(0,1/2,1/2)$ for tetragonal structure. The absence of energy gap in DOS shown in Figure 3 confirms the metallic nature of NdTe₂.

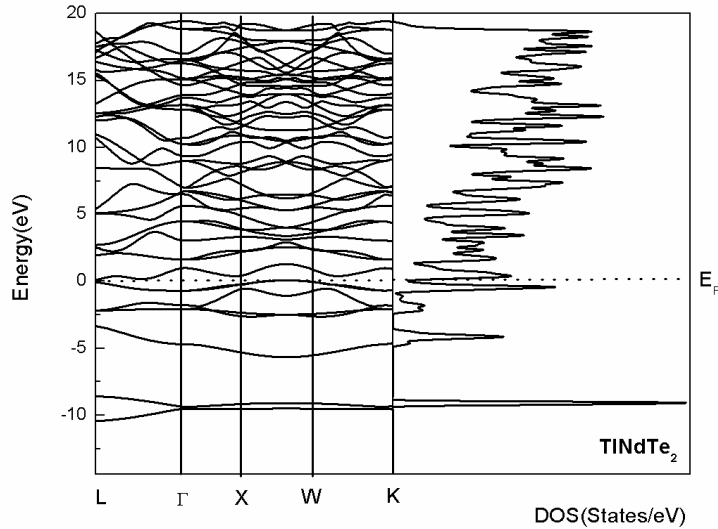


Figure 4. The energy bands and corresponding total DOS of TiNdTe₂

The calculated band structure and density of states of TiNdTe₂ (L2₁) are presented in Figure 4. The symmetry points are L(1/4,1/4,1/4), Γ (0,0,0), X(0,1/2,0), W(1/4,1/2,0) and K(1/3,1/3,0) for face-centered cubic structure. In Figure 4, band structures of TiNdTe₂ show the semi-metallic character. The general methodology for the calculation of the band structure is established by the same process.

The partial DOS (PDOS) are very useful as they give information on hybridization and the orbital character of the states. From the PDOS we are able to identify the angular momentum character of the different structure.

The calculated PDOS is presented in Figure 5 for NdTe₂. It is recognized that the lowest band as arising from a bonding state of s character. Nd-p, Nd-d, Te-p and Te-d states are more dominated than both s-states. The next two bands intersect each other at several points in the Brillouin Zone (BZ). The total DOS at Fermi level is nearly $n(E_f)=2.98$ states/eV/unit cell.

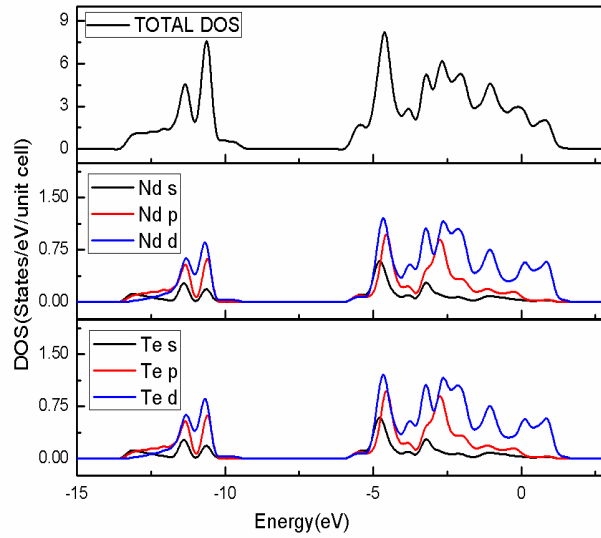


Figure 5. Electronic density of states of NdTe_2 in tetragonal structure

Calculation of the electron density of states for TlNdTe_2 shows that Tl-d, Te-d and Nd-d orbitals have been given much more contribution according to its p and d orbitals in Figure 6. On the other hand, contribution of Te-p orbital is quite much. From Figures 5 and 6, one can see that the positions of Fermi level for NdTe_2 and TlNdTe_2 are all near a minimum of DOS. This supports their ductile behaviors.

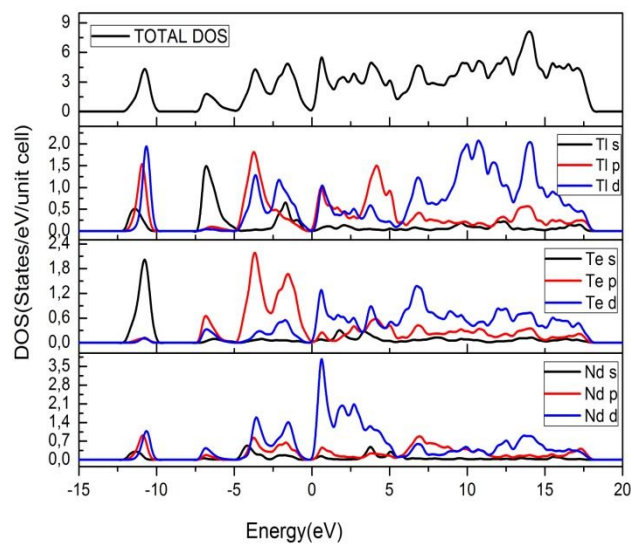


Fig. 6. Electronic density of states of TlNdTe_2 in the Heusler structure

In order to mention the relationship between the electronic structure and ductility properties of related compounds, the electron localization function (ELF) is exploited. It is essential to consider that ELF is more appropriate than the electronic charge density in describing chemical bonds due to the fact that it amplifies the bonding properties of a given electron distribution and permits comparison of the bonding of different electron distributions on an certain scale [49]. The ELF value is scaled between 0 and 1. The formula of ELF is given by

$$ELF = \frac{1}{1 + \left(\frac{D(\vec{r})}{D_h(\vec{r})} \right)^2} \quad (4)$$

with

$$D(\vec{r}) = \frac{1}{2} \sum_{i=1}^n X_i \nabla_{\vec{r}} \nabla_{\vec{r}'} \rho(\vec{r}, \vec{r}') \Big|_{\vec{r}=\vec{r}'} - \frac{1}{8} \frac{|\nabla n(\vec{r})|^2}{n(\vec{r})} \quad (5)$$

and

$$D_h(\vec{r}) = \frac{3}{10} (3\pi^2)^{2/3} n(\vec{r})^{5/3} \quad (6)$$

where ρ is the first-order reduced (spin integrated) density matrix. $D(\vec{r})$ is the von Weizsäcker kinetic-energy functional and $D_h(\vec{r})$ is the kinetic-energy density of a uniform electron gas with a spin density equal to the local value of $n(\vec{r})$. In the case of exceeding delocalization, assumed ELF values close to zero while in the case of high localization, ELF values close to one.

In the regions where the valance charge distribution is similar to the homogeneous electron gas, the ELF gets to 0.5. The electron localization function is calculated using VASP (Vienna Ab-initio Simulation Package), the periodic plane-wave density functional code of Kresse and Hafner [51] and Kresse and Furthmüller [51]. The structural calculations are performed by VASP, which employs pseudopotentials

and the generalized gradient approximation (GGA) to model the contribution of the exchange correlation to the total energy and the valence electron density distribution. The lattice parameters for NdTe₂ are in good agreement with experimental study.

In order to visualize the nature of the bonding character, charge density distributions are obtained for NdTe₂ and TlNdTe₂. To determine the charge densities in symmetry points at energy-band diagrams, charge density contour plots are needed. In each case the contour lines are drawn at a constant interval. In Figure 7, the bonding charge density plotted in the (110) plane. It can be easily seen that a significant overlapping can be observed between Nd and Te bonding, indicating covalent bonding in the electronegativity between Nd and Te bonding.

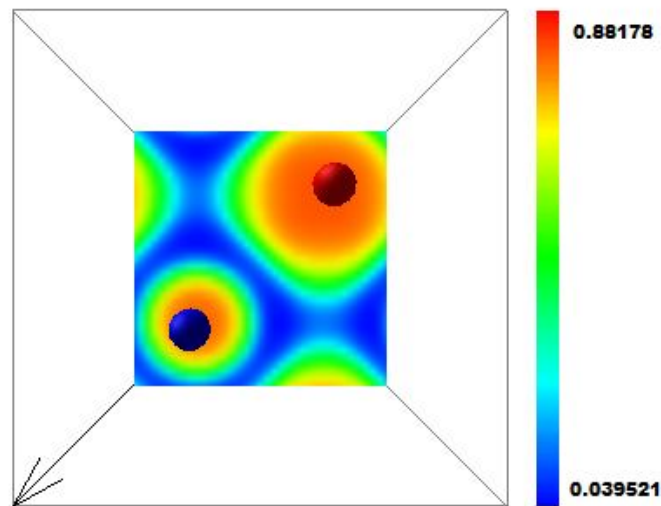


Figure 7. ELF contour plot of NdTe₂ on the (110) plane

The red sphere shows Nd element and blue sphere shows Te element that exhibits rectangular regions along the bond path and blue colored areas in the interstice with low electron localization (ELF=0.039) compared to the bulk of the interionic space where ELF reaches respectively 0.805 for Nd and 0.759 for Te in Figure 7.

All these features are identified in the plots of the total charge densities with ELF contour plots in Figure 7 and 8. Pseudo-wave functions which disappear at the

position of the ion are used for calculation. The charge is mostly concentrated in the region among atoms.

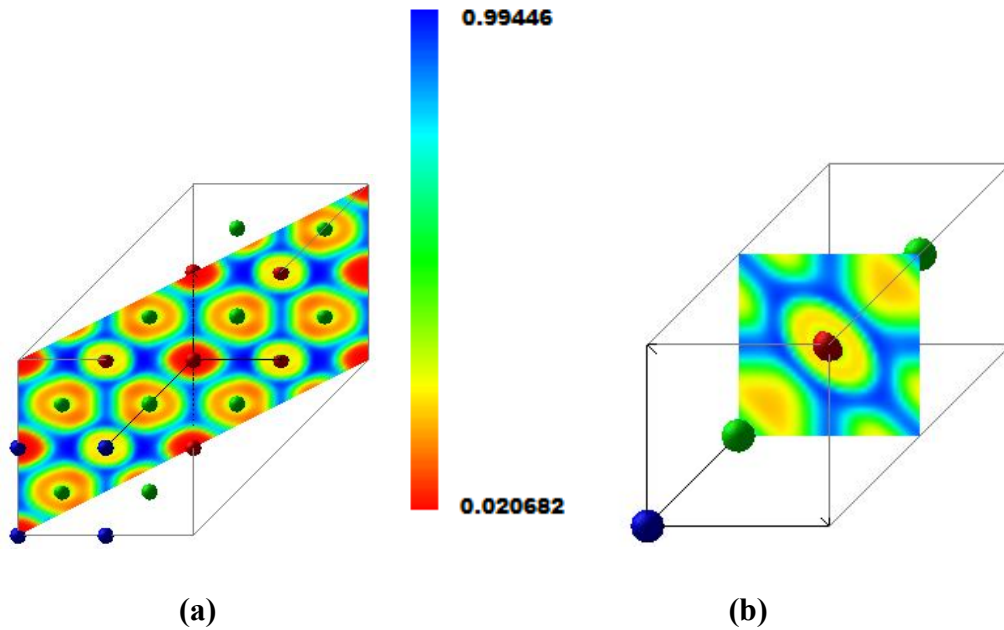


Figure 8. (a) Cross-section (with 45° angle) of ELF contour plot of TiNdTe₂ (b) ELF contour plot of TiNdTe₂ on the (110) plane in 3D

Contour plot of electron localization function is presented for TiNdTe₂ in Figure 8 in which blue spheres are Ti, red spheres are Nd and the green spheres are Te. In Figure 8 (a), ELF contour plot of TiNdTe₂ is given in 45° angle. ELF values are given nearly 0.994 for Ti, 0.593 for Nd and 0.121 for Te respectively. There is one neodymium atom in the middle of unit cell as shown in Figure 8 (b). It is also seen that the TiNdTe₂ has semi-metallic character.

The ELF contour plot of NdTe₂ and ELF contour plot of TiNdTe₂ with ELF isosurfaces where all data has the same value are presented in Figure 9.

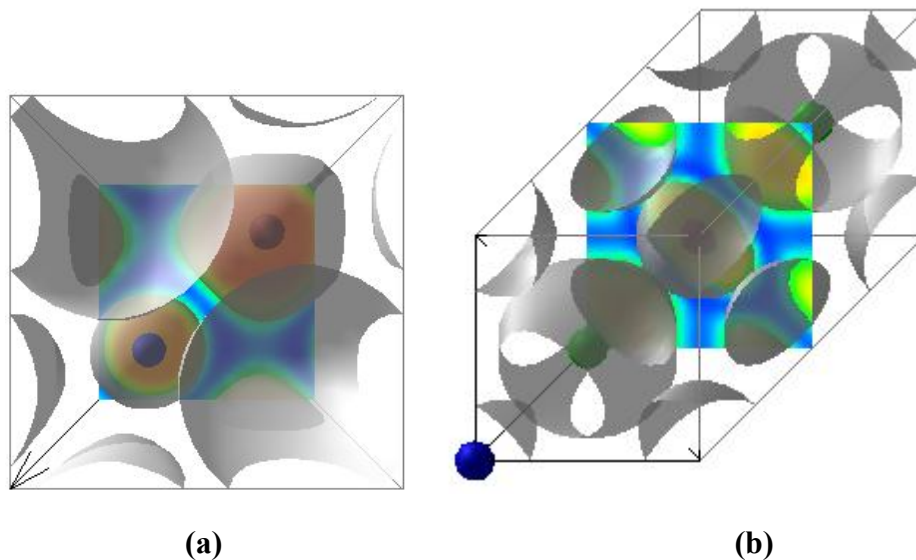


Fig. 9. (a) ELF contour plot of NdTe_2 with ELF isosurfaces (b) ELF contour plot of TiNdTe_2 with ELF isosurfaces

The only one arbitrary ELF isosurface (gray colored) displays on the map is chosen at value of 0.829. The ELF isosurfaces are topologically similar to electron density gradient domains and the topology of the negative Laplacian of the electron density $[L(r)]$. The two-dimensional electron density difference maps provide information about electron probability density above and below the two-dimensional plane. Therefore, ELF isosurface maps might be useful tool for visual of the location of bonded and lone pair electrons [52-54].

CONCLUSIONS

In summary, we have performed GGA calculations to obtain the structural, elastic and electronic properties of $\text{NdTe}_2(\text{C38})$ and $\text{TiNdTe}_2(\text{L2}_1)$. Lattice constants, bulk modulus and its pressure derivative, second-order elastic constants (C_{ij}), isotropic shear modulus (G), B/G , Zener anisotropy factor (A), Young's modulus (E), Poisson's ratio (ν) and Kleinman parameter are calculated for these compounds. Brittle/ductile behaviors are determined. In electronic calculations, calculated band structure and total DOS and partial DOS are presented. ELF contour plots and ELF isosurfaces are discussed.

Acknowledgement: This study is supported by Ankara University Research Project Unit (12B4343020).

REFERENCES

- [1] C.G. Duan, R.F. Sabirianov, W.N. Mei, P.A. Dowben, S.S. Jaswal, E.Y. Tsymbal. Electronic, magnetic and transport properties of rare-earth monpnictides. *J. Phys. Condens. Matter.*, 2007, **19**: 315220.
- [2] S. Lebegue, S. Svane, M. Katsnelson, I. Lichtenstein, O. Eriksson. Multiplet effects in the electronic structure of light rare-earth metals. *Physical Rev. B*, 2006, **74**: 045114.
- [3] G. Pagare, P.S. Sanyal, P.K. Jha. High-pressure behaviour and elastic properties of heavy rare-earth Gd monpnictides. *Journal of Alloys and Compounds*, 2005, **398**: 16-20.
- [4] C.J.M. Rooymans. *Structural Investigations on Some Oxides and Other Chalcogenides at Normal and Very High Pressures (Philips Research Reports)*, Philips, Eindhoven, 1968.
- [5] A. Chatterjee, A.K. Singh, A. Jayaraman. Pressure-Induced Electronic Collapse and Structural Changes in Rare-Earth Monochalcogenides, *Phys. Rev. B*, 1972, **6**: 2285.
- [6] A. Jayaraman, A.K. Singh, A. Chatterjee, S. Usha Devi. Pressure-volume relationship and pressure-induced electronic and structural transformations in Eu and Yb monochalcogenides. *Phys. Rev. B*, 1974, **9**: 2513.
- [7] V.V. Shchennikov, N.N. Stepanov, I.A. Smirnov, A.V. Golubkov. Thermoelectric power and resistivity of samarium monochalcogenides at ultrahigh pressure. *Sov. Phys.-Solid State*, 1988, **30**: 1785.
- [8] U. Benedict, W.B. Holzapfel, in: K.A. Gschneidner, L. Eyring, G.H. Lander, G.R. Choppin (Eds.). *Handbook on the Physics and Chemistry of Rare Earths*, North-Holland, Amsterdam, 1993.
- [9] V.A. Sidorov, N.N. Stepanov, L.G. Khvostantsev, O.B. Tsiok, A.V. Golubkov, V.S. Oskotski, I.A. Smirnov. Intermediate valency state of samarium chalcogenides under high pressure. *Semicond. Sci. Technol.*, 1989, **4**: 286.
- [10] O.B. Tsiok, V.A. Sidorov, V.V. Bredikhin, L.G. Khvostantsev. Compressibility and electronic transport properties of SmSe and SmTe at the pressure induced valence transition. *Solid State Commun.*, 1991, **79**: 227.
- [11] T. Le. Bihan, S. Darracq, S. Heathman, U. Benedict, K. Mattenberger, O. Vogt. Phase transformation of the monochalcogenides SmX (X : S, Se, Te) under high pressure. *J. Alloy. Compd.*, 1995, **226**: 143.

- [12] J.M. Leger, R. Epain, J. Lories, D. Ravot, J. Rossat-Mignod. Anomalous behavior of CeTe under high pressures. *Phys. Rev. B*, 1983, **28**: 7125.
- [13] J.M. Leger, D. Ravot, J. Rossat-Mignod. Volume behaviour of CeSb and LaSb up to 25 GPa. *J. Phys. C Solid State Phys.*, 1984, **17**: 4935.
- [14] N. Mori, Y. Okayama, H. Takahashi, Y. Haga, T. Suzuki. Neutron scattering investigations of magnetic ordering and crystal field excitations in CeAs under high pressure. *Physica B*, 1993, **444**: 186-188.
- [15] U. Benedict. Comparative aspects of the high-pressure behaviour of lanthanide and actinide compounds. *J. Alloy. Compd.*, 1995, **223**: 216-225.
- [16] I. Shirotni, K. Yamanashi, J. Hayashi, Y. Tanaka, N. Ishimatsu, O. Shimomura, T. Kikegawa. Phase transitions of LnAs (Ln = Pr, Nd, Sm, Gd, Dy and Ho) with NaCl-type structure at high pressures. *J. Phys. Condens. Matter*, 2001, **13**: 1939.
- [17] I. Shirotni, K. Yamanashi, J. Hayashi, N. Ishimatsu, O. Shimomura, T. Kikegawa. Pressure-induced phase transitions of lanthanide monoarsenides LaAs and LuAs with a NaCl-type structure. *Solid State Commun.*, 2003, **127**: 573.
- [18] A. Svane, G. Santi, Z. Szotek, W.M. Temmerman, P. Strange, M. Horne, G. Vaitheeswaran, V. Kanchana, L. Petit, H. Winter. Electronic structure of Sm and Eu chalcogenides. *Phys. Status Solidi B*, 2004, **241**: 3185.
- [19] D. Singh, M. Rajagopalan, A.K. Bandyopadhyay. Band structure calculation and structural stability of high pressure phases of EuSe. *Solid State Commun.*, 1999, **112**: 39.
- [20] D. Singh, M. Rajagopalan, M. Husain, A.K. Bandyopadhyay. High pressure band structures and structural stability of EuS. *Solid State Commun.*, 2000, **115**: 323.
- [21] D. Singh, V. Srivastava, M. Rajagopalan, M. Husain, A.K. Bandyopadhyay. High-pressure band structure and structural stability of EuTe. *Phys. Rev. B*, 2001, **64**: 115110.
- [22] P. Larson, Walter R. L. Lambrecht. Electronic structure of rare-earth nitrides using the LSDA+*U* approach: Importance of allowing 4*f* orbitals to break the cubic crystal symmetry. *Phys. Rev. B*, 2007, **75**: 045114.
- [23] C.G. Duan, R. F. Sabiryanov, Jianjun Liu, W. N. Mei, P. A. Dowben and J. R. Hardy. Strain Induced Half-Metal to Semiconductor Transition in GdN. *Phys. Rev. Lett.*, 2005, **94**: 237201.
- [24] V.N. Antonov, B.N. Harmon, A.N. Yaresko. Electronic structure of mixed-valence semiconductors in the LSDA+*U* Sm monochalcogenides approximation. *Phys. Rev. B*, 2002, **66**: 165208.

- [25] G. Vaitheeswaran, V. Kanchana, M. Rajagopalan. Theoretical study of LaP and LaAs at high pressures. *J. Alloy. Compd.*, 2002, **336**: 46.
- [26] P. Pandit, V. Srivastava, M. Rajagopalan, S.P. Sanyal. Pressure-induced electronic and structural phase transformation properties in half-metallic PmN: A first-principles approach. *Physica B*, 2008, **403**: 4333.
- [27] Y. Wenlong, Y. Shihong, Y. Dunbo, L. Kuoshe, L. Hongwei, L. Yang, Y. Hongchuan. Influence of gadolinium on microstructure and magnetic properties of sintered NdGdFeB magnets. *Journal of Rare Earths*, 2012, **30**: 133-136.
- [28] Cristiano C. Bastos, Ricardo O. Freire, Gerd B. Rocha, Alfredo M. Simas. Sparkle model for AM1 calculation of neodymium(III) coordination compounds. *J. Photochemistry and Photobiology A: Chemistry*, 2006, **177**: 225–237.
- [29] Th. Böker, R. Severin, A. Müller, C. Janowitz, R. Manzke. Band structure of MoS₂, MoSe₂, and α -MoTe₂: Angle-resolved photoelectron spectroscopy and *ab initio* calculations. *Phys. Rev. B*, 2001, **64**: 235305.
- [30] Y. Mogulkoc, Y.O. Ciftci, K. Colakoglu. Structural, elastic, electronic and thermodynamic properties of Nd₂Te via first principle calculations. *J. Optoelectron. Adv. Mater.*, 2011, **13**: 946-95.
- [31] Klaus Stöwe. Crystal structure, magnetic properties and band gap measurements of NdTe_{2-x} ($x=0.11(1)$). *Zeitschrift für Kristallographie*, 2001, **216**: 0044-2968.
- [32] E.M. Godzhaev, K.D. Orudzhev, V.A. Mamedov and F.S. Mirzoeva. TlNdSe₂ – TlInSe₂ and TlInTe₂ – TlNdTe₂ Systems. *Izv. Akad. Nauk SSSR, Neorg. Mater.*, 1981, **17**: 1388–1391.
- [33] P. Hohenberg, W. Kohn. Inhomogeneous Electron Gas. *Phys. Rev.*, 1964, **136**: 864.
- [34] W. Kohn, L.J. Sham. Self-Consistent Equations Including Exchange and Correlation Effects, *Phys. Rev.*, 1965, **140**: 1133.
- [35] A.D. Becke, K.E. Edgecombe. A simple measure of electron localization in atomic and molecular systems. *J. Chem. Phys.*, 1990, **92**: 5397.
- [36] G. Kresse, J. Furthmüller. Efficient iterative schemes for *ab initio* total-energy calculations using a plane-wave basis set. *Phys. Rev. B*, 1996, **54**: 11169.
- [37] G. Kresse, J. Furthmüller. Efficiency of *ab-initio* total energy calculations for metals and semiconductors using a plane-wave basis set. *Compt. Mater. Sci.*, 1996, **6**: 15.
- [38] P.E. Blöchl. Projector augmented-wave method. *Phys. Rev. B*, 1994, **50**: 17953.
- [39] G. Kresse, J. Joubert. From ultrasoft pseudopotentials to the projector augmented-wave method. *Phys. Rev. B*, 1999, **59**: 1758.

- [40] J. Perdew, K. Burke, M. Ernzerhof. Generalized Gradient Approximation Made Simple. *Phys. Rev. Lett.*, 1996, **77**: 3865.
- [41] F.D. Murnaghan. The Compressibility of Media under Extreme Pressures. *Proc. Natl. Acad. Sci. USA*, 1944, **30**: 5390.
- [42] J. Mehl. Pressure dependence of the elastic moduli in aluminum-rich Al-Li compounds. *Phys. Rev. B*, 1993, **47**: 2493.
- [43] O.H. Nielsen, R.M. Martin. First-Principles Calculation of Stress. *Phys. Rev. Lett.*, 1983, **50**: 697.
- [44] Y. Le Page, P. Saxe. Symmetry-general least-squares extraction of elastic data for strained materials from *ab initio* calculations of stress. *Phys. Rev. B*, 2002, **65**: 104104.
- [45] S.Q. Wang, H.Q. Ye. First-principles study on elastic properties and phase stability of III–V compounds. *Phys. Status Solidi B*, 2003, **240**: 45.
- [46] M. Born and K. Huang. *Dynamical Theory of Crystal Lattices*, Clarendon, Oxford, 1956.
- [47] B. Mayer, H. Anton, E. Bott, M. Methfessel, J. Sticht, and P.C. Schmidt. Ab-initio calculation of the elastic constants and thermal expansion coefficients of Laves phases. *Intermetallics*, 2003, **11**: 23.
- [48] W.A. Harrison, *Electronic Structure and Properties of Solids*, New York: Dover, 1989.
- [49] L. De Santis and R. Resta. Electron localization at metal surfaces. *Surf. Sci.*, 2000, **450**: 126.
- [50] G. Kresse, J. Hafner. *Ab initio* molecular dynamics for liquid metals. *Phys. Rev. B*, 1993, **47**: 558–561.
- [51] G. Kresse and J. Furthmüller. Efficient iterative schemes for *ab initio* total energy calculations using a plane-wave basis set. *Phys. Rev. B*, 1996, **54**: 11169.
- [51] R.F.W. Bader, S. Johnson, T.H. Tang, P.L.A. Popelier. The Electron Pair. *J. Phys. Chem.*, 1996, **100**: 15398-15415.
- [52] A. Kirfel, T. Lippmann, P. Blaha, K. Schwarz, D.F. Cox, K.M. Rosso, G.V. Gibbs. Electron density distribution and bond critical point properties for forsterite, Mg(2)SiO(4), determined with synchrotron single crystal X-ray diffraction data. *Phys. Chem. Min.*, 2005, **32**: 301-313.
- [53] G.V. Gibbs, D.F. Cox, N.L. Ross, T.D. Crawford, J.B. Burt, K.M. Rosso. Experimental and theoretical bond critical point properties for model electron density distributions for earth materials. *Phys. Chem. Min.*, 2005, **32**: 208-221.